IEEE Access
Multidisciplinary | Rapid Review | Open Access Journal

Received 5 August 2024, accepted 28 August 2024, date of publication 4 September 2024, date of current version 24 September 2024.

Digital Object Identifier 10.1109/ACCESS.2024.3454295

RESEARCH ARTICLE

Micro Linear Ultrasonic Motor With a Hall Sensor-Based Feedback Control System

SHUNSUKE IZUHARA[1], (Member, IEEE), AND TOMOAKI MASHIMO[2],(Member, IEEE)
[1]Department of Mechanical and Electrical Systems Engineering, Kyoto University of Advanced Science, Kyoto 615-8577, Japan
[2]Graduate School of Natural Science and Technology, Okayama University, Okayama 700-8530, Japan

Corresponding author: Shunsuke Izuhara (izuhara.shunsuke@kuas.ac.jp)

This work was supported in part by the Grant-in-Aid for Japan Society for the Promotion of Science (JSPS) KAKENHI under Grant JP19J21092 and Grant JP23K13247, and in part by the Japan Science and Technology Agency (JST) Fusion Oriented Research for disruptive Science and Technology (FOREST) Program under Grant JPMJFR212G.

ABSTRACT We propose a one-millimeter-scale linear ultrasonic motor and its feedback control system with a Hall sensor. The size of the stator measures 1.6 mm in height, 1.6 mm in width, and 0.3 mm in thickness, and there is a hole with a diameter of 0.6 mm at the center, which is one of the smallest linear motors reported to date. A similar-sized Hall sensor detects the displacement of the slider inserted into the stator hole for position control. In this paper, we build the prototype motor and evaluate its basic performance measures, such as electrical impedance characteristics and mechanical output characteristics. The optimization of the preload between the stator and slider has improved the thrust force of the motor to the maximum value of 7.6 mN, resulting in a higher force-to-volume ratio than existing miniature linear motors. We combine the motor with a Hall sensor having a similar scale to the motor and construct a feedback system with a burst-wave control. The feedback control succeeded in removing the steady-state error that remains in the open-loop system.

INDEX TERMS Ferroelectric materials, microactuators, piezoelectric actuators.

I. INTRODUCTION

Micro linear actuators are a key technology for numerous applications, ranging from mobile and camera devices to minimally invasive treatment and diagnosis devices. Various driving principles have been attempted for micro linear actuators [1], [2], such as electromagnetic force [3], electrostatic force [4], and electrochemical reactions [5]; however, low force-to-volume ratio of these actuators limits their further deployment. An actuator with a high force-to-volume ratio is shape memory alloy (SMA), but its short stroke length is an inherent problem [6].

Piezoelectric actuators have the potential to become micro motors due to their simple structure and high force density [7], [8], [9], [10]. The design of micro linear motors requires an appropriate driving principle for miniaturization, such as vibration modes. Typical driving principles for miniature linear piezoelectric actuators include the combination of L1 and B2 vibration modes [11], [12], [13], [14] and the stick-slip principle [15], [16]. These piezoelectric actuators can be miniaturized to a scale of 4 – 10 mm and are practically used for camera focus mechanisms (e.g., [13], [15]). However, their driving principle requires a long stator in the traveling direction, which limits further miniaturization. To further minimize linear piezoelectric actuators, several researchers have studied the simultaneous excitation of two vibration modes [17], [18], [19] and the selective excitation of various resonant vibration modes [20], [21] as driving principles. These stators, which range in size from 2.6 to 5 mm, provide practical output for moving lenses or sensors. However, further miniaturization of these actuators has not been studied, although smaller linear actuators are demanded.

Once a small piezoelectric linear motor has been realized, a sensor and control strategy are required for the motor control. The sensor must also be of similar size to the motor to exploit the motor size. The most well-known distance sensors are infrared sensors that use triangulation [22] and ultrasonic

The associate editor coordinating the review of this manuscript and approving it for publication was Hassen Ouakad.

sensors that use the time-of-flight principle [23], but it is difficult in principle to make these sensors smaller. Hall sensors, which measure a varying magnetic field and convert it into an electrical signal, have been commercialized with a one-millimeter scale (e.g. [24]). If the slider of a linear motor is magnetized, there is a possibility that the Hall sensors can detect the slider position. Reference [25], [26] However, the feasibility of a control system using such a tiny linear motor and sensor has not been studied.

In this study, we build a micro linear ultrasonic motor with a square stator that measures 1.6 mm in height, 1.6 mm in width, and 0.3 mm in thickness. It uses the simultaneous excitation of two vibration modes as a driving principle. Although this principle has been proposed with much larger stators [27], it is not clear, whether one-millimeter-scale stators work has not been studied. Another issue to be mentioned in this paper is controlling such a tiny linear motor with a displacement sensor. For making a closed-loop, a tiny sensor that can measure the displacement of the linear motor must be selected without enlarging the whole size. A large number of miniature linear motors have been proposed, but how to integrate them into control systems has not been discussed.

The main contributions of this paper are summarized as follows.

1) The micro linear ultrasonic motor, which is one of the smallest linear motors, is built and characterized. The resulting motor has a higher force-to-volume ratio than existing miniature linear motors.
2) A tiny Hall sensor, which is used as a displacement sensor, is integrated into the motor system, constructing a closed loop. The feedback system can improve the steady-state characteristics of the motor.

The remainder of this paper is organized as follows. Section II describes the driving principle of the micro linear ultrasonic motor. In section III, a tiny stator is prototyped and its electrical characteristics are evaluated using impedance analysis. The dynamic and static characteristics of the micro ultrasonic motor are evaluated in section IV. Finally, section V demonstrates a feedback control of the micro linear ultrasonic motor and a similar-scale Hall sensor.

II. DRIVING PRINCIPLE

Fig. 1(a) shows the design and driving principle of the micro linear ultrasonic motor. The stator consists of a metallic square cuboid with a center hole and four piezoelectric elements bonded to its sides. The top and bottom of the piezoelectric elements (PZTs) employ the thickness-shear piezoelectric effect (15 mode), while the left and right employ the expansion piezoelectric effect (31 mode). The thickness-shear effect excites the bending vibration of the plate (axial vibration mode), as shown in Fig. 1(c). In the bending vibration, the hole moves back and forth in the axial direction of the slider (thickness direction of the stator). The expansion effect repeats expansion and contraction,

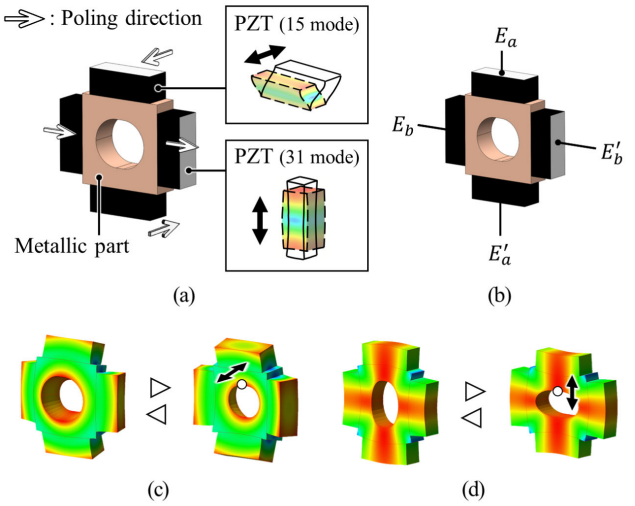

FIGURE 1. (a) Stator structure of the micro linear ultrasonic motor and (b) voltages applied to the stator. The vibration modes of the driving principle are (c) axial vibration mode and (d) radial vibration mode.

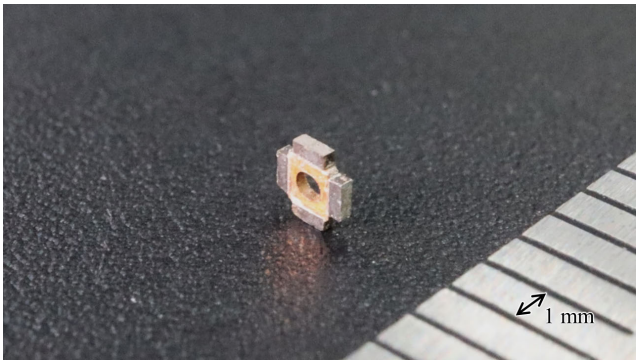

FIGURE 2. Prototype stator of the micro linear ultrasonic motor.

exciting the longitudinal vibration shown in Fig. 1(d) (radial vibration mode). This mode deforms the hole in the radial direction (direction in the width and height of the stator). These vibration modes have independent natural frequencies, which can have the same value by designing the dimensions of the stator. The agreement of their natural frequencies enables the excitation of the two vibration modes at the same frequency.

To excite the two modes simultaneously, four AC voltages are applied to the stator as shown in Fig. 1(b). They are denoted as $E_a = A_E \sin(2\pi f_E t)$, $E'_a = -A_E \sin(2\pi f_E t)$, $E_b = A_E \cos(2\pi f_E t)$, and $E'_b = -A_E \sin(2\pi f_E t)$, where A_E and f_E are the amplitude and frequency of the applied voltage, respectively. The frequency f_E is adjusted to correspond to the natural frequency of the two modes. When the four voltages are applied, the axial and radial vibration modes are excited with a phase difference of $\pi/2$. The combination of the axial and radial vibration modes produces an elliptical motion, which transfers the vibration energy to the slider inserted in the stator hole by friction.

III. STATOR PROTOTYPE AND EVALUATION

A. STATOR PROTOTYPE

The dimensions of the metallic part and the piezoelectric elements have been designed using finite element method (FEM) analysis so that the stator can excite the axial and radial modes simultaneously. The FEM analysis software (FEMTET, Murata Software Co., Tokyo, Japan) shows the mode shapes and their resonant frequencies. We defined the width and height of the metallic part to be 1.0 mm. They are made of hard piezoelectric material with dimensions of 0.8 mm × 0.3 mm and a thickness of 0.3 mm. When the thickness of the metallic part is 0.29 mm, the axial and radial vibration modes are given at 470 kHz. Fig. 2 shows a prototype stator of the micro linear ultrasonic motor. The dimensions are the same as those of the FEM described above. Four piezoelectric elements (C-213, Fuji Ceramics Co., Fujinomiya, Japan) are bonded to the metal using conductive epoxy adhesive. The components are fabricated using conventional machining processes. For example, the metallic part is milled from a bronze plate and the piezoelectric elements are cut using a dicing saw, a process commonly used in semiconductor fabrication.

B. IMPEDANCE ANALYSIS

The axial and radial vibration modes generated by the prototype stator are examined by an impedance analyzer (IM3570, Hioki E. E. Co., Japan). These modes can be selectively distinguished by changing the connections of wires. To select the axial vibration mode, an impedance analyzer is connected to the top and bottom sides. For the radial vibration mode, the impedance analyzer is connected to the right and left sides. Fig. 3 shows how the impedance and phase of the prototype stator behave when the frequency f_E varies from 400 to 600 kHz. The axial vibration mode and the radial vibration mode appear at 464.0 kHz (Fig. 3(a)) and 460.7 kHz (Fig. 3(b)), respectively. Fig. 3(c) summarizes the measurement results for resonant frequencies f_r, anti-resonant frequencies f_a, coupling factor k, and quality factor Q. (See Appendix for how to estimate the coupling coefficient k and the quality factor Q.) The coupling coefficient k of the axial vibration mode is slightly lower than that of the radial vibration mode; however, the quality factor Q of the axial vibration mode is more than three times higher than that of the radial vibration mode. One of the reasons is that the quality factor of the thickness-shear piezoelectric effect is higher than that of the expansion piezoelectric effect.

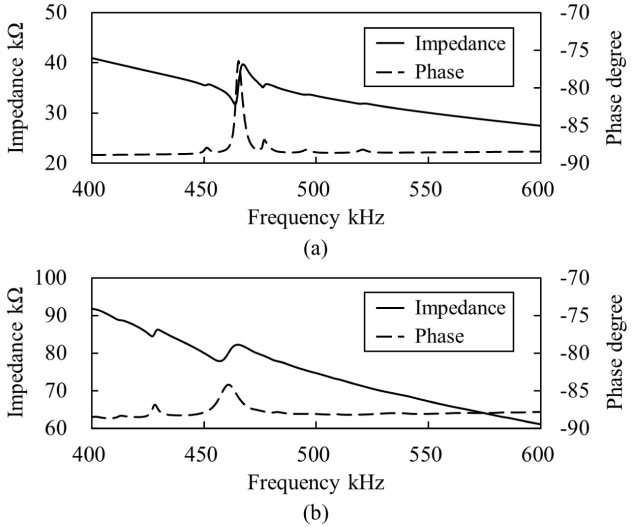

	f_r kHz	f_a kHz	k %	Q
Axial vibration mode	464.0	467.5	12.2	206.8
Radial vibration mode	460.7	465.2	13.8	55.8

(c)

FIGURE 3. Frequency characteristic of the current measured by impedance analysis. The change in the current by (a) the axial vibration mode and (b) the radial vibration mode. (c) Experimental characteristics when the stator generates axial and radial vibration modes.

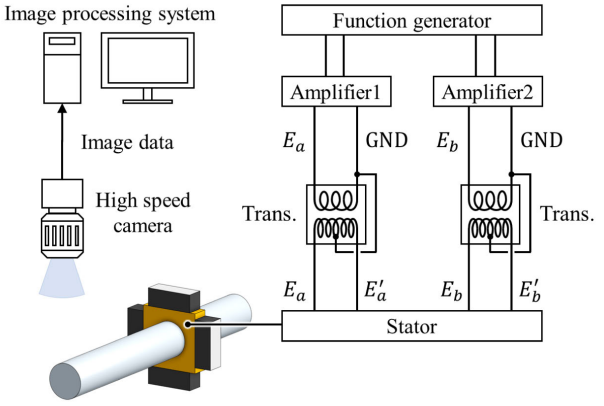

FIGURE 4. Experimental setup for evaluating how the preload changes the motor output.

IV. PERFORMANCE EVALUATION

A. EXPERIMENTAL SETUP

This subsection describes the experimental setup to evaluate the characteristics of the micro linear ultrasonic motor. The right side of Fig. 4 shows the motor drive system. A two-channel function generator (WF1974, NF Corp., Yokohama, Japan) is used to generate two voltages with sine and cosine signals. These two signals are then amplified to voltages with an amplitude of A_E by power amplifiers (HSA4052, NF Corp.). Thus, these devices generate the voltages $E_a = A_E \sin(2\pi f_E t)$ and $E_b = A_E \cos(2\pi f_E t)$. Two transformers placed after the amplifiers invert the voltages E_a and E_b to the voltages $E'_a = -A_E \sin(2\pi f_E t)$ and $E'_b = -A_E \cos(2\pi f_E t)$, respectively. The four voltages, E_a, E'_a, E_b, and E'_b are applied to the piezoelectric elements of the stator. The amplitude A_E and frequency f_E of the voltages can be adjusted using the wave generator and amplifiers.

When voltages are applied, the slider inserted into the stator begins to move. The movement of the slider from the

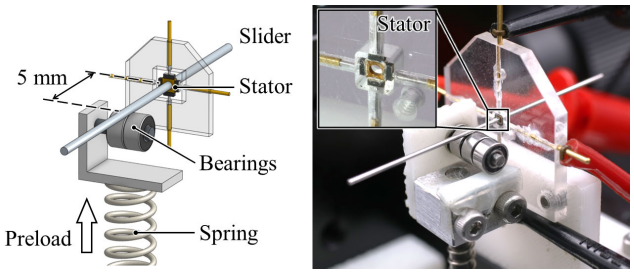

FIGURE 5. Experimental setup for evaluating how the preload changes the motor output.

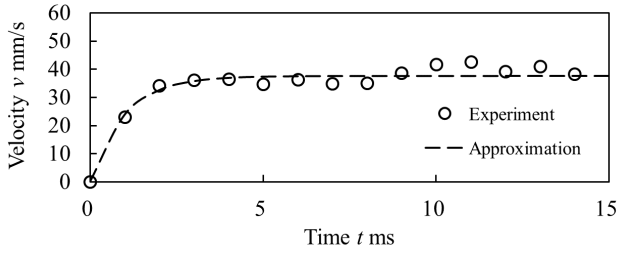

FIGURE 6. The transient response of the micro linear ultrasonic motor.

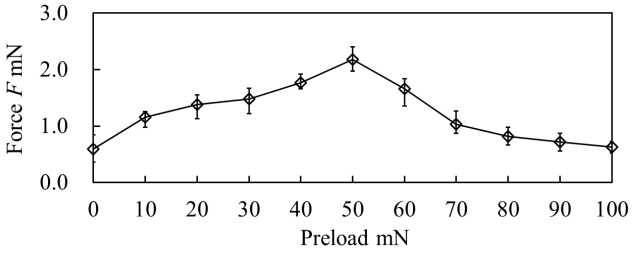

FIGURE 7. Relationship between the thrust force and the applied preload. For each case, the performance is evaluated five times and the averaged values are plotted. The error bars indicate maximum and minimum value from five tests of one preload value.

transient state to the steady state is captured using a camera, as shown on the left side of Fig. 4. The camera is a high-speed camera with an image resolution of 640 × 480 pixels at 1000 fps (VW-9000, Keyence Co., Tokyo, Japan). Velocity and acceleration are calculated by differentiating the image data with time. The output thrust force is estimated from the calculated acceleration and the mass of the slider in the following experiments.

Fig. 5 shows the mechanical hardware of the experimental setup. The stator is fixed at the center of the jig, and its sides are supported by contact probes that serve as electrodes for applying voltages. A slider, a cylindrical stainless steel shaft with a diameter of 0.610 mm, a length of 40 mm, and a weight of approximately 94.0 mg, is inserted into the stator hole. In this setup, the preload between the stator and slider can be adjusted by a spring force to give the motor a higher thrust force. As shown on the left in Fig. 5, the preload is applied to the slider by a tiny bearing connected to a spring. The distance between the center of the bearing and the stator is 5 mm. The tiny bearing allows the slider to move linearly without friction. The preload value can be estimated from the spring displacement and spring constant.

B. TRANSIENT RESPONSE

The transient response shows the dynamic behavior of the micro linear ultrasonic motor. The motion of common ultrasonic motors behaves as a first-order system [28]. When the motor generates force F and moves a slider with a mass of m, the velocity v of the slider is obtained as

$$m\dot{v} + cv = F, \tag{1}$$

where c denotes the damping coefficient.

The transient response of the micro linear ultrasonic motor is measured experimentally. In this experiment, the input voltages of $f_E = 480$ kHz and $A_E = 50$ V_{peak} are applied, and the preload of 50 mN is set by adjusting the spring force. (Here, f_E is slightly higher than the resonance frequency f_r obtained in III-B because the resonance frequency changes due to the existence of the slider.) Fig. 6 shows the experimental result. The linear velocity reaches a steady state at about 2 ms, and the average steady-state velocity is approximately 37.6 mm/s. The thrust force of $F = 2.31$ mN is estimated from the initial acceleration and the mass of the slider. The dashed line shows the approximation curve obtained using (1). In the estimation, the mass and force are the actual values and the damping coefficient $c = 0.095$ Ns/m is obtained.

C. CHARACTERIZATION

The optimal preload can be clarified by examining the relationship between the thrust force and preload. This relationship can be estimated using the Coulomb friction model, which involves elliptical motion that moves a slider through point contact [29]. For a given preload N between the stator and slider, the thrust force F produced by the motor can be expressed using the Coulomb friction model as:

$$F = \mu_d N, \tag{2}$$

where μ represents the friction coefficient. However, it is important to note that this model has a limited range. While the thrust force increases linearly with the preload, excessive preload hinders the movement of the slider.

Fig. 7 shows the behavior of the thrust force when the preload is varied. The thrust force increases with preload at the low preload and peaks at 50 mN; a maximum thrust force of approximately 2.2 mN is obtained. Beyond the peak, the thrust force decreases because a higher preload suppresses the vibration of the stator. This relationship between the thrust force and preload is observed in the characteristics of friction-drive ultrasonic motors.

As the fundamental characteristics, we examine how the thrust force and linear velocity behave by changing the voltage. During the experiments, the preload that peaks the thrust force ($N = 50$ mN) is constant.

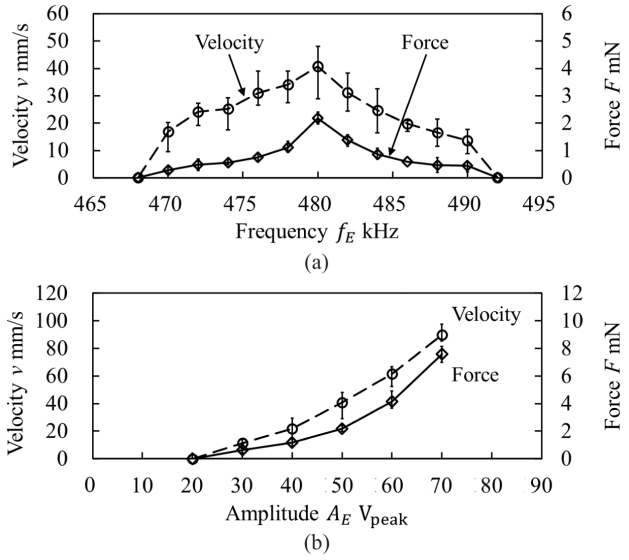

FIGURE 8. (a) Frequency and (b) amplitude characteristics of the motor output. For each case, the performance is evaluated five times and the averaged values are plotted in these figures. The error bars indicate the maximum and minimum values.

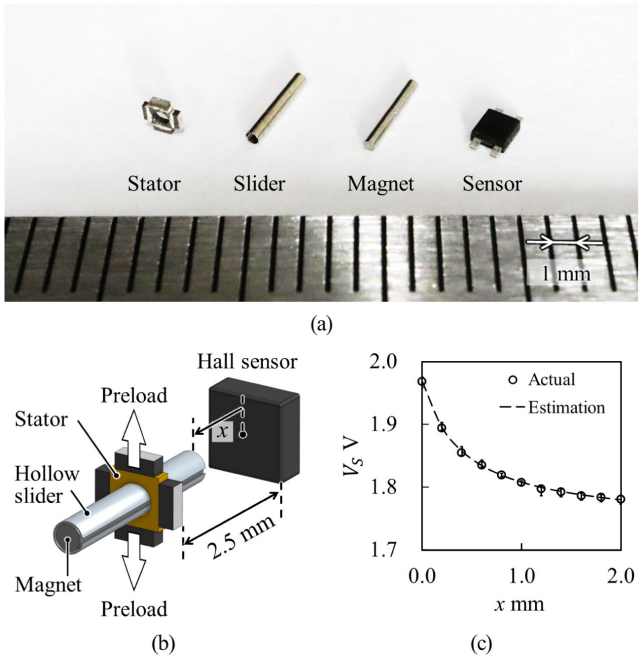

FIGURE 9. (a) Components of the motor. From left: the stator, the hollow cylindrical slider, a cylindrical magnet, and a Hall sensor. (b) The motor-sensor system using a hollow slider with a magnet and a Hall sensor. (c) The relationship between the displacement of the slider x and the sensor output V_C.

Fig. 8(a) shows the frequency characteristics at the constant amplitude ($A_E = 50\ V_{peak}$). A peak thrust force of approximately 2.2 mN and peak velocity of approximately 40.7 mm/s are obtained at 480 kHz. Fig. 8(b) shows the amplitude characteristics at the constant frequency ($f_E = 480$ kHz). The slider starts to move at an amplitude larger than 20 V_{peak}, and the force and velocity increase with the amplitude. At the highest amplitude ($A_E = 70\ V_{peak}$), the thrust force is approximately 7.6 mN and the velocity is approximately 89.9 mm/s.

V. FEEDBACK CONTROL

A. COMPONENTS FOR CONTROL SYSTEM

How to construct the feedback system is another interest in this study. The system requires a sensor that can detect the displacement of the slider of the micro linear ultrasonic motor for making a closed-loop. A sensor must be as small as the one-millimeter-scale linear motor so as not to enlarge the total size. Taking the size into account, we selected a Hall sensor that outputs a voltage proportional to one axial component of the magnetic field by Hall effect; a small type of Hall sensor is commercially available.

Implementation of the magnet into the linear motor is a design issue to make the Hall sensor work as the linear displacement sensor. To mention this issue, we take the advantage of that the slider of the proposed motor can be hollow. In other words, a magnet that the Hall sensor detects can be placed inside the slider, without adding extra parts and without enlarging the mechanism. The other important aspect of designing the slider is the preload between the stator and slider. (In the previous section, the preload is applied by a tiny bearing and spring, but this mechanism is too large to be used with the micro linear ultrasonic motor.) To make the slider have a preload generation mechanism without enlarging the size, we employ a thin hollow cylinder with a slit as the slider [27]. When the slider, the diameter of which is slightly larger than the diameter of the stator hole, is inserted into the stator hole, a restoring force acting as a preload is generated.

Fig. 9(a) shows the components for constructing the feedback system: stator, slider, magnet, and Hall sensor, from the left. The diameter of the stator hole is 0.627 mm. The slider measures a diameter of 0.629 mm, a length of 4 mm, and a thickness of 25 μ m. It has a slit about 0.1 mm wide, which equals an angle of 18.6°. The slider is made of nickel and weighs about 3 mg. The slider is produced by electroforming, a metal-forming process that involves the precise deposition of a conductive metal layer that allows the creation of hollow cylinders with micron order tolerances. The tiny magnet is a solid cylinder made of stainless steel with a diameter of 0.6 mm and a length of 4 mm, magnetized using a neodymium magnet with a magnetic flux of 0.5 T. The Hall sensor is a commercially available product (HG-166A-2U, Asahi Kasei Microdevices Corporation, Japan) and its size is 1.5 mm × 1.5 mm × 0.6 mm.

Fig. 9(b) shows the arrangement of the linear motor and the Hall sensor. When the slider is inserted into the stator hole, the preload acts at the stator-slider interface. The Hall sensor is positioned in the direction of slider displacement. When the slider moves linearly, the magnetic field varies. The Hall sensor detects the change in the magnetic field and provides an analog voltage output.

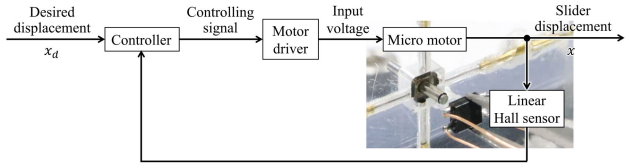

FIGURE 10. Control system for the micro linear motor.

It is possible to estimate the position of the slider by the calibration between the output voltage of the sensor and the slider displacement. Fig. 9(c) shows how the sensor output behaves as the displacement x varies.

When x is zero, the sensor signal takes a peak value. As x increases, the sensor signal decreases. When x exceeds 1 mm, the change in the output voltage becomes gradual. Therefore, we determined that the range of the position control for the demonstration is within the range of 0 to 1.0 mm. The displacement error estimated by the Hall sensor at $x = 1$ mm is about ± 0.05 mm.

B. CONSTRUCTION OF FEEDBACK SYSTEM

To achieve precise control of the slider displacement, a proportional control (P-control) is used. The proportional controller is designed such that the thrust force F is proportional to the difference between the desired displacement x_d and the actual displacement x. This can be expressed as:

$$F = k_p(x_d - x). \tag{3}$$

Here, k_p represents the proportional gain. By substituting (3) into (1), the equation of motion that describes the behavior of the displacement x is derived. This equation is a second-order system:

$$m\ddot{x} + c\dot{x} + k_p x = k_p x_d, \tag{4}$$

In this equation, $k_p x_d$ is a virtual elastic term that brings the actual displacement to a stop at the desired position. Higher values of k_p allow the slider to reach the desired displacement more quickly. However, if the value of k_p is set too high, it can cause overshoot and make the system unstable.

Fig. 10 shows the flow of the signal and the power in the feedback system that consists of the motor, sensor, motor driver (the system of the function generator and amplifiers), and microcontroller. Once the desired displacement x_d is inputted into the microcontroller (Arduino Uno, Arduino Co., Italy), the microcontroller computes the error between the desired displacement x_d and the actual displacement x, and determines the control signal. The control signal is a pulse-width modulation (PWM) signal with a duty ratio, which changes in proportion to the extent of the error. In response to the control signal, the motor driver turns high-frequency voltages on and off. This on-and-off high-frequency voltage with the duty ratio is called *burst wave* [30]. (The burst wave control is similar to the PWM control used in electromagnetic motors, although the voltage types differ.) The position of the slider is detected by the Hall sensor, and the output voltage of the Hall sensor is converted into actual displacement in the microcontroller based on the measurement results shown in Fig. 9(c).

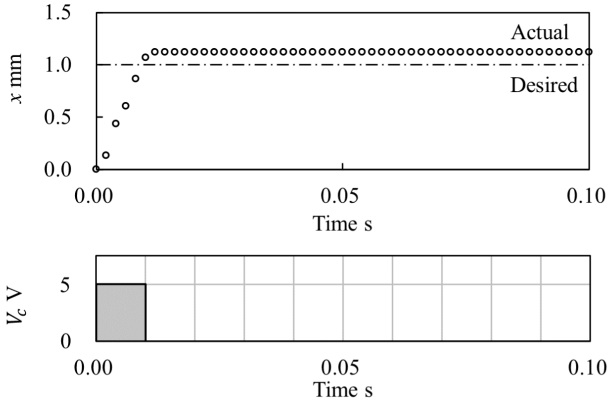

FIGURE 11. When the bang-bang control is applied, transient response of the hollow linear slider and time history of the cotrol signal V_c.

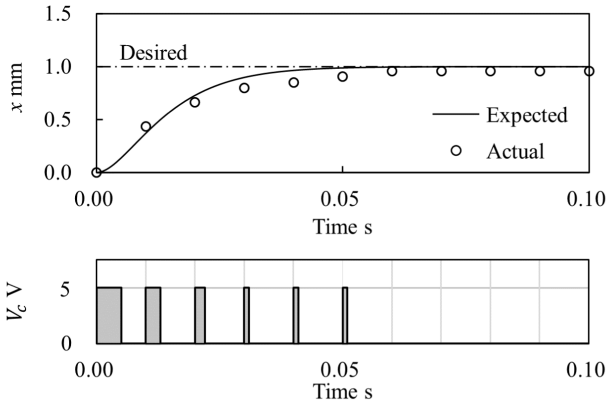

FIGURE 12. When the P-control is applied, transient response of the hollow linear slider and time history of the cotrol signal V_c.

C. DEMONSTRATION

To demonstrate the effectiveness of using the feedback control, the transient response using the P-control is compared with that using the bang-bang control. During the experiments, the desired displacement is 1 mm and the applied voltages are constant ($A_E = 50\ \mathrm{V_{peak}}, f_E = 480$ kHz). The control cycle of this system is 1 ms.

The bang-bang control simply turns on and off the slider motion. When the desired displacement (dash-dotted line) is given, the controller sends a signal to drive the motor. When the slider reaches the desired displacement, the controller sends the signal to stop the motor. Fig. 11 shows the transient response with bang-bang control. The slider displacement x reaches the desired displacement within 10 ms. When the desired displacement is satisfied, the controller sends a signal to stop the motion. However, the slider moves over the desired displacement and remains a steady-state error.

This is because of the delay that comes from the inertia and the communication speed.

The P-control changes the duty ratio to the error between x_d and x. In the motor-sensor system, when the proportional gain k_p is set to 3.6, the damping ratio of the system is 1 (critically damped). To ensure stable operation without oscillation, the system is set to $k_p = 3.4$. The burst wave period is 10 ms and the maximum duty ratio is 0.5 because a larger duty ratio causes an overshoot. Fig. 12(a) shows the behavior of the slider with P-control. As the displacement x approaches the target, the controller reduces the duty ratio of the burst wave, as shown in Fig. 12(b). At the start of the motion, the duty ratio is large. When the slider approaches the desired, the duty ratio becomes small. The actual behavior with the burst-wave control is in good agreement with the estimated curve and succeeded in achieving the desired position without overshooting.

VI. CONCLUSION

In this study, we proposed a micro linear ultrasonic motor and evaluated its performance. The stator measures 1.6 mm *times* 1.6 mm *times* 0.3 mm, achieved by using the thickness shear piezoelectric effect and the expansion piezoelectric effect. This motor is the smallest linear ultrasonic motor reported to date [2], [9], [10]. By designing an optimal preload, the output force of the solid cylindrical slider was improved to approximately 7.6 mN at a voltage amplitude of 70 V_{peak}. In addition, it was confirmed that accurate positioning of the slider can be achieved by constructing a control system using a slider with a magnet and a Hall sensor.

Table 1 shows a comparison of existing miniature linear ultrasonic motors with stator side lengths of 5 mm or less. The stator volume of the proposed motor is less than 1 cubic millimeter and the thrust per stator volume is relatively high. In addition, the proposed motor generates the practical force without any additional mechanisms (e.g., preload and linear guide mechanism) to move the slider. These characteristics make it suitable for next-generation devices such as endoscopes or micromanipulators.

In order to implement the micro linear ultrasonic motor in practical devices, several problems such as stabilizing the thrust force, improving the efficiency, and clarifying the resolution must be solved. A key idea for solving these problems is to optimize the contact condition between the stator and the slider, which involves coating the slider with a suitable material with an optimal coefficient of friction. Another interesting aspect of this study is a modeling approach used to analyze the details of the micro linear ultrasonic motor. This type of model could help to understand the behavior on a very small scale, leading to greater accuracy, control, and robustness for practical applications.

TABLE 1. Comparison with miniature linear ultrasonic motors.

Design	Stator size mm	Max. force mN	Force per volume mN/mm^3
Proposed motor	1.6×1.6×0.29	7.6	10.2
$L_1 - B_2$ [14]	1.12×1.63×3.93	56	7.81
Cuboid motor [19]	2.6×2.6×2.2	20	1.34
Baltan motor [20]	2×3.25×3.67	44	1.84
Two-layer micromotor [21]	2×2×5	294	14.7
Miniswys SA [31]	3×0.75×4.5	50	4.93

APPENDIX
COUPLING COEFFICIENT AND QUALITY FACTOR

The coupling coefficient k and quality factor Q are important parameters for evaluating the stator quality. The coupling coefficient is the ratio of the mechanical energy consumed to the supplied electrical energy. A stator with a higher coupling coefficient can be driven with a lower voltage. It can be approximated from the relationship between the resonance and antiresonance in the impedance curve [32]:

$$k = \sqrt{\frac{f_a^2 - f_r^2}{f_a^2}} \tag{5}$$

where f_r and f_a are the resonant and antiresonant frequencies, respectively. Quality factor Q is a dimensionless parameter that expresses the underdamped stator. The quality factor of the stator evaluates the sharpness of the resonance in the designed stator. A higher quality factor indicates larger vibration amplitudes with low damping. It is calculated from the curve of the current using the full width at half maximum method [33]:

$$Q = \frac{f_r}{\Delta f} \tag{6}$$

where Δf is the half-width of the current curve.

REFERENCES

[1] H. Ishihara, F. Arai, and T. Fukuda, "Micro mechatronics and micro actuators," *IEEE/ASME Trans. Mechatronics*, vol. 1, no. 1, pp. 68–79, Mar. 1996.
[2] T. Mashimo and S. Izuhara, "Review: Recent advances in micromotors," *IEEE Access*, vol. 8, pp. 213489–213501, 2020.
[3] C.-L. Hsieh, C.-S. Liu, and C.-C. Cheng, "Design of a 5 degree of freedom–voice coil motor actuator for smartphone camera modules," *Sens. Actuators A, Phys.*, vol. 309, Jul. 2020, Art. no. 112014.
[4] N. Tas, J. Wissink, L. Sander, T. Lammerink, and M. Elwenspoek, "Modeling, design and testing of the electrostatic shuffle motor," *Sens. Actuators A, Phys.*, vol. 70, nos. 1–2, pp. 171–178, Oct. 1998.
[5] T. F. Otero, M. T. Cortés, and G. V. Arenas, "Linear movements from two bending triple-layers," *Electrochimica Acta*, vol. 53, no. 3, pp. 1252–1258, Dec. 2007.
[6] J. Mohd Jani, M. Leary, A. Subic, and M. A. Gibson, "A review of shape memory alloy research, applications and opportunities," *Mater. Design*, vol. 56, pp. 1078–1113, Apr. 2014.
[7] T. Morita, "Miniature piezoelectric motors," *Sens. Actuators A, Phys.*, vol. 103, no. 3, pp. 291–300, Feb. 2003.
[8] B. Watson, J. Friend, and L. Yeo, "Piezoelectric ultrasonic micro/milli-scale actuators," *Sens. Actuators A, Phys.*, vol. 152, no. 2, pp. 219–233, Jun. 2009.
[9] Y. Peng, Y. Peng, X. Gu, J. Wang, and H. Yu, "A review of long range piezoelectric motors using frequency leveraged method," *Sens. Actuators A, Phys.*, vol. 235, pp. 240–255, Nov. 2015.
[10] X. Tian, Y. Liu, J. Deng, L. Wang, and W. Chen, "A review on piezoelectric ultrasonic motors for the past decade: Classification, operating principle, performance, and future work perspectives," *Sens. Actuators A, Phys.*, vol. 306, May 2020, Art. no. 111971.

[11] T. Funakubo and Y. Tomikawa, "Characteristics of 10 mm multilayer L1-F2Mode vibrator and application to a linear motor," *Jpn. J. Appl. Phys.*, vol. 42, no. 5, pp. 3002–3006, May 2003.
[12] H.-P. Ko, H. Jeong, and B. Koc, "Piezoelectric actuator for mobile auto focus camera applications," *J. Electroceram.*, vol. 23, nos. 2–4, pp. 530–535, Oct. 2009.
[13] *Nano Usm: Fast and Smooth Focusing at Your Fingertips*. Accessed: Feb. 23, 2024. [Online]. Available: https://snapshot.canon-asia.com/article/eng/ef-lens-technology-nano-usm-revolutionises-your-photos
[14] J. J. Zhang, W. D. Diao, K. Fan, Z. Q. Wang, R. Q. Shi, and Z. H. Feng, "A miniature standing wave linear ultrasonic motor," *Sens. Actuators A, Phys.*, vol. 332, Dec. 2021, Art. no. 113113.
[15] R. Yoshida, Y. Okamoto, and H. Okada, "Development of smooth impact drive mechanism (2nd report)," *J. Jpn. Soc. for Precis. Eng.*, vol. 68, no. 4, pp. 536–541, 2002.
[16] T. Yokose, H. Hosaka, R. Yoshida, and T. Morita, "Resonance frequency ratio control with an additional inductor for a miniaturized resonant-type SIDM actuator," *Sens. Actuators A, Phys.*, vol. 214, pp. 142–148, Aug. 2014.
[17] D. Sun, S. Wang, J. Sakurai, K.-B. Choi, A. Shimokohbe, and S. Hata, "A piezoelectric linear ultrasonic motor with the structure of a circular cylindrical stator and slider," *Smart Mater. Struct.*, vol. 19, no. 4, Apr. 2010, Art. no. 045008.
[18] W.-H. Lee, C.-Y. Kang, D.-S. Paik, B.-K. Ju, and S.-J. Yoon, "Butterfly-shaped ultra slim piezoelectric ultrasonic linear motor," *Sens. Actuators A, Phys.*, vol. 168, no. 1, pp. 127–130, Jul. 2011.
[19] S. Izuhara and T. Mashimo, "Design and evaluation of a micro linear ultrasonic motor," *Sens. Actuators A, Phys.*, vol. 278, pp. 60–66, Aug. 2018.
[20] J. Friend, Y. Gouda, K. Nakamura, and S. Ueha, "A simple bidirectional linear microactuator for nanopositioning–the 'Baltan' microactuator," *IEEE Trans. Ultrason., Ferroelectr., Freq. Control*, vol. 53, no. 6, pp. 1160–1168, Jun. 2006.
[21] X. Li, P. Ci, G. Liu, and S. Dong, "A two-layer linear piezoelectric micromotor," *IEEE Trans. Ultrason., Ferroelectr., Freq. Control*, vol. 62, no. 3, pp. 405–411, Mar. 2015.
[22] S.-S. Kim, C. Young, and B. Mizaikoff, "Miniaturized mid-infrared sensor technologies," *Anal. Bioanal. Chem.*, vol. 390, no. 1, pp. 231–237, Jan. 2008.
[23] Z. Qiu, Y. Lu, and Z. Qiu, "Review of ultrasonic ranging methods and their current challenges," *Micromachines*, vol. 13, no. 4, p. 520, Mar. 2022.
[24] G. Boero, M. Demierre, P.-A. Besse, and R. S. Popovic, "Micro-Hall devices: Performance, technologies and applications," *Sens. Actuators A, Phys.*, vol. 106, nos. 1–3, pp. 314–320, Sep. 2003.
[25] T. Kanda, H. Maeda, and K. Suzumori, "A micro ultrasonic motor controlled by using a built-in micro magnetic encoder," in *Proc. IEEE/ASME Int. Conf. Adv. Intell. Mechatronics*, Jul. 2010, pp. 1029–1034.
[26] *Website of New Scale Technologies*. Accessed: Aug. 5, 2024. [Online]. Available: https://www.newscaletech.com/micro-motion-modules/m3-l-linear-smart-actuators/
[27] S. Izuhara and T. Mashimo, "Design and characterization of a thin linear ultrasonic motor for miniature focus systems," *Sens. Actuators A, Phys.*, vol. 329, Oct. 2021, Art. no. 112797.
[28] Q. Lv, Z. Yao, and X. Li, "Modeling and experimental validation of a linear ultrasonic motor considering rough surface contact," *Smart Mater. Struct.*, vol. 26, no. 4, Apr. 2017, Art. no. 045023.
[29] T. Mashimo and K. Terashima, "Experimental verification of elliptical motion model in traveling wave ultrasonic motors," *IEEE/ASME Trans. Mechatronics*, vol. 20, no. 6, pp. 2699–2707, Dec. 2015.
[30] T. Mashimo, S. Izuhara, S. Arai, Z. Zhang, and H. Oku, "High-speed visual feedback control of miniature rotating mirror system using a micro ultrasonic motor," *IEEE Access*, vol. 8, pp. 38546–38553, 2020.
[31] *Website of the Company Miniswys*. Accessed: Jul. 26, 2022. [Online]. Available: https://www.miniswys.com
[32] Y. Liu, W. Chen, J. Liu, and X. Yang, "A high-power linear ultrasonic motor using bending vibration transducer," *IEEE Trans. Ind. Electron.*, vol. 60, no. 11, pp. 5160–5166, Nov. 2013.
[33] J. Wu, Y. Mizuno, and K. Nakamura, "Polymer-based ultrasonic motors utilizing high-order vibration modes," *IEEE/ASME Trans. Mechatronics*, vol. 23, no. 2, pp. 788–799, Apr. 2018.

SHUNSUKE IZUHARA (Member, IEEE) received the Ph.D. degree in mechanical engineering from Toyohashi University of Technology, Japan, in 2022. He is currently an Assistant Professor with the Nagamori Institute of Actuators, Kyoto University of Advanced Science, Kyoto, Japan. His research interest includes micro piezoelectric actuators.

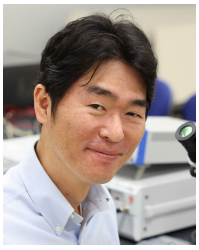

TOMOAKI MASHIMO (Member, IEEE) received the Ph.D. degree in mechanical engineering from Tokyo University of Agriculture and Technology, Tokyo, Japan, in 2008. From 2008 to 2010, he was a Robotics Researcher with the Robotics Institute, Carnegie Mellon University, Pittsburgh, PA, USA. After being an Assistant Professor (Tenure-Track) with Toyohashi University of Technology, Toyohashi, Japan, in 2011. He became an Associate Professor, in 2016. Since 2022, he has been a Professor with the Graduate School of Natural Science and Technology, Okayama University. His research interests include piezoelectric actuators and robotic applications.